electronics

Article

Simple Learning-Based Robust Nonlinear Control of an Electric Pump for Liquid-Propellant Rocket Engines

Mohammad Jafari [1,*], Mahmut Reyhanoglu [1,*] and Zhandos Kozhabek [2]

1 Robotics Engineering Program, Columbus State University, Columbus, GA 31907, USA
2 Department of Space Engineering and Technology, Almaty University of Power Engineering and Telecommunications, Almaty 050013, Kazakhstan; z.kozhabek@aues.kz
* Correspondence: jafari_mohammad@columbusstate.edu (M.J.); reyhanoglu_mahmut@columbusstate.edu (M.R.)

Abstract: This paper presents a robust nonlinear control strategy for an electric pump for liquid-propellant rocket engines. In order to compensate for model uncertainties and disturbances, a gradient-descent-based simple learning control strategy is employed that minimizes the cost function defined on the error dynamics of the nonlinear system. Detailed stability analysis for the nonlinear system is provided. Computer simulation results are included to demonstrate the effectiveness of the nonlinear control method using an electric pump model consisting of a brushless permanent-magnet direct current (DC) motor and a centrifugal pump. In particular, it is shown that by employing the developed nonlinear controller, the mass flow rate can be successfully kept at a certain level, can be changed instantly from one level to another (immediate decrease or increase), or can be changed linearly/nonlinearly, gradually, and continually for a certain period.

Keywords: learning control; electric pump; nonlinear control

check for updates

Citation: Jafari, M.; Reyhanoglu, M.; Kozhabek, Z. Simple Learning-Based Robust Nonlinear Control of an Electric Pump for Liquid-Propellant Rocket Engines. *Electronics* **2023**, *12*, 3527. https://doi.org/10.3390/electronics12163527

Academic Editors: Nakkeeran Kaliyaperumal and Ahmed Abu-Siada

Received: 27 July 2023
Revised: 13 August 2023
Accepted: 18 August 2023
Published: 21 August 2023

1. Introduction

Fuel consumption management is one of the key tasks in the development and operation of rocket engines. This is especially important for liquid-propellant rocket engines, which are used in launch systems and space missions, where every gram of fuel is of great importance. Various monitoring and diagnostic systems are used to control fuel consumption in liquid rocket engines. Control of the fuel consumption in such engines is achieved by controlling the turbopump or the electric pump unit that pumps fuel from tanks to the combustion chamber [1,2]. Controlling the fuel flow through the pump reduces fuel consumption and improves engine efficiency. One method for controlling the fuel flow is to use variable speed pumps [3–6]. This allows one to adjust the fuel consumption depending on the current operating conditions of the engine. For example, at low rocket speed, fuel consumption can be reduced to extend the flight time [7]. In addition, it is important to control the speed of rotation of the blades. This allows you to achieve the best pump efficiency and reduce fuel consumption. Fuel quality control also plays an important role. The presence of impurities and foreign particles can affect pump performance and increase fuel consumption. Therefore, it is necessary to regularly check the quality of the fuel and clean it from impurities [8].

Generally, turbopump-type engines for rockets, which use liquid propellant, send an oxidant and a fuel at high pressure to a main combustor by using a high-temperature gas generated from a gas generator, thereby generating thrust. An interesting alternative to turbopump systems is to use battery-powered electric motors to drive the centrifugal pumps, which are commonly known as electric pumps [1].

Electric pumps in liquid-propellant engines provide a powerful alternative to using gas generator–turbine systems or turbopump systems. Moreover, electric pumps have high efficiency and a simplified structure that does not require high development costs, making them ideal for space applications including satellite propulsion systems [9,10].

With the recent advances in battery technology, electric pumps have become viable for launch systems as well [11]. Details on the design of liquid-propellant rocket engines that employ electric pumps can be found in [12]. The reliability of the propellant supply system for such engines was noted in [13–15].

The management of fuel consumption in liquid rocket engines with an electric pump unit is an important task that allows you to increase the efficiency of the engine and reduce fuel consumption. For this, a control system is used that controls the speed of rotation of the pump and adjusts it to the required operating mode of the engine [6,16,17]. The regulation of the pump speed as part of a liquid-propellant rocket engine with an electric pump unit is a very important process since the efficiency of the engine and its durability depend on it. Therefore, the control system must be reliable and accurate, which will ensure the stability of the entire system as a whole.

The design of linearization-based controllers for an electric pump in a deep-throttling rocket engine was studied in [16], where the effect of nonlinearity was analyzed using a gap metric. The linearization-based PID controllers are known to be effective only in the vicinity of the operating point. In [16], this drawback is circumvented via a gain scheduling approach. While these linearization-based methods are simple, their effectiveness in mitigating modeling uncertainties and external disturbances is limited. In general, to address the challenges associated with system nonlinearities, modeling uncertainties, and external disturbances, several broad classes of control techniques are available in the literature. To name a few, one can mention the sliding mode control (SMC) [18], learning-based model predictive control (MPC) [19], neural network (NN)-based learning control [20], fuzzy control (FC) [21], feedback linearization control (FLC) [22], backstepping control (BC) [23], and biologically inspired control (BIC) [24] techniques. These techniques have their advantages over the others, therefore, it is very common to design a controller by combining two or more of these techniques [25–27].

Among these, one of the commonly used control approaches is the feedback linearization control methodology. While traditional FLC-based techniques are greatly utilized, their performance might degrade when dealing with system nonlinearities, modeling uncertainties, and external disturbances. To enhance the traditional FLC-based techniques, one can utilize the capability of the learning-based methods. In this paper, we propose to use the simple learning (SL) control approach that we developed in our previous work [28–30] for the control of an electric pump consisting of a battery-powered direct current (DC) motor and a centrifugal pump. It must be noted that this nonlinear control approach eliminates the need to use disturbance estimators while providing robustness against uncertainties and disturbances.

The organization of this paper is as follows: Section 2 introduces the model of the electric pump considered in this paper. In Section 3, the SL-based nonlinear robust control law is developed. In Section 3.1, the update rules for the controller gains and disturbance estimates are derived. Section 3.2 provides proof of the closed-loop stability. The satisfactory performance of the proposed method is illustrated by providing numerical simulations of the electric pump in Section 4, and finally, Section 5 includes the conclusions and comments on future research directions.

2. Mathematical Model

In this paper, we develop a mathematical model of the speed control system for the electric pump unit of a liquid-propellant rocket engine using a brushless electric motor and a lithium polymer battery.

The electric pump considered in this paper has a battery-powered direct current (DC) motor and a centrifugal pump as seen in Figure 1. Consider a brushless permanent-magnet DC motor. Applying Kirchhoff's voltage law to the armature circuit yields

$$
\begin{aligned}
V_a &= L_a \frac{dI_a}{dt} + R_a I_a + V_b \\
V_b &= K_v \omega_m
\end{aligned}
\tag{1}
$$

where V_a and I_a, respectively, denote the armature voltage (which is considered the control input variable) and the armature current, R_a and L_a, respectively, are the armature resistance and the armature inductance, and V_b is the back electromotive force, which is proportional to the angular speed ω_m through the motor voltage constant K_v. The mechanical balance is described by

$$\begin{aligned} J_m \frac{d\omega_m}{dt} + B_m\omega_m &= \tau_m - \tau_l \\ \tau_m &= K_t I_a \end{aligned} \tag{2}$$

Here τ_m and τ_l, respectively, denote the motor driving torque and the load reaction torque, J_m and B_m, respectively, are the moment of inertia and viscous friction coefficient, and K_t is the motor torque constant.

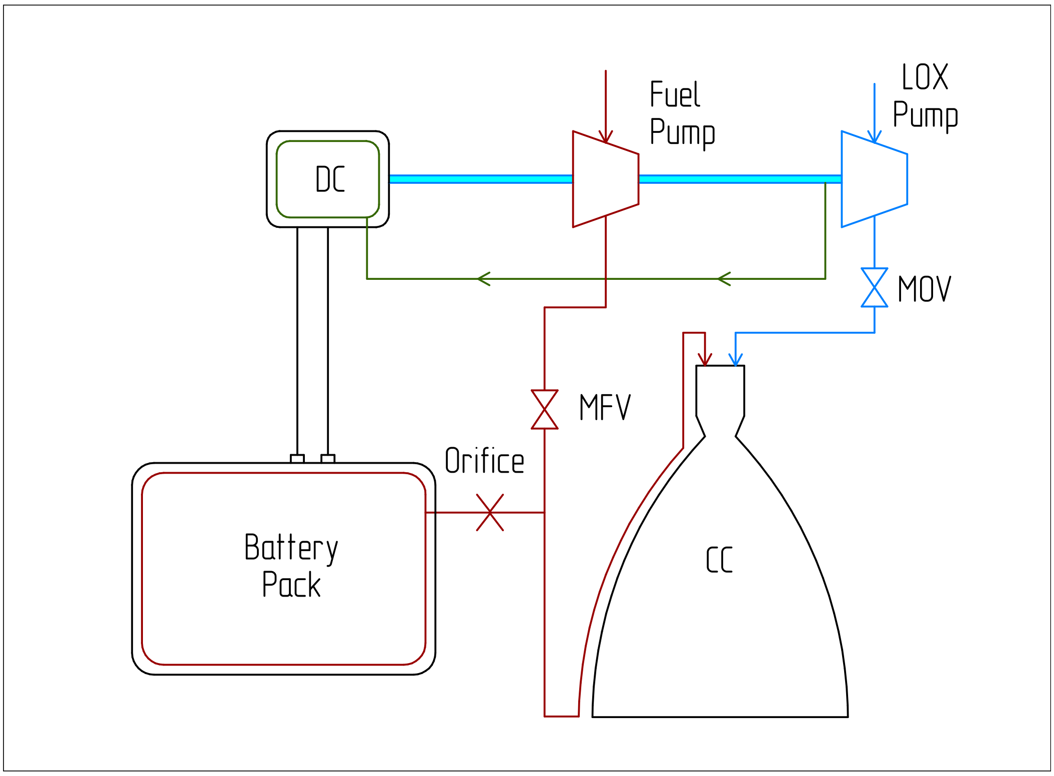

Figure 1. Schematic representation of the electric pump.

The load torque by which the pump is driven can be expressed as

$$\tau_l = Kn^2 \tag{3}$$

where K is a constant and n is the rotational speed, which can be expressed as

$$n = \frac{60\omega_m}{2\pi} \tag{4}$$

The electric pump dynamics can then be expressed as

$$\begin{aligned} \frac{dI_a}{dt} &= -\frac{R_a}{L_a}I_a - \frac{K_v}{L_a}\omega_m + \frac{1}{L_a}V_a \\ \frac{d\omega_m}{dt} &= \frac{K_t}{J_m}I_a - \frac{B_m}{J_m}\omega_m - \frac{K}{J_m}n^2 \end{aligned} \tag{5}$$

Let $\dot{m}_r$ and n_r, respectively, denote the reference mass flow rate and the reference rotational speed. Assuming that the rotational speed of the pump is proportional to the mass flow rate of the pump, the rotational speed of the pump can be computed by

$$n = \dot{m}\frac{n_r}{\dot{m}_r} \tag{6}$$

Then electric pump dynamics Equation (5) can be re-expressed as

$$\begin{aligned} \frac{dI_a}{dt} &= a_1 I_a + a_2 \dot{m} + bV_a \\ \frac{d\dot{m}}{dt} &= a_3 I_a + a_4 \dot{m} + c\dot{m}^2 \end{aligned} \tag{7}$$

where

$$\begin{aligned} a_1 &= -\frac{R_a}{L_a}, & a_2 &= -\frac{\pi n_r K_v}{30\dot{m}_r L_a} \\ a_3 &= \frac{30\dot{m}_r K_t}{\pi n_r J_m}, & a_4 &= -\frac{B_m}{J_m} \\ b &= \frac{1}{L_a}, & c &= -\frac{30 n_r K}{\pi \dot{m}_r J_m} \end{aligned} \tag{8}$$

Selecting $u = V_a$ as the control input and $y = n$ as the output, the following nonlinear input–output equation can be obtained:

$$\ddot{y} - (a_1 + a_4)\dot{y} + (a_1 a_4 - a_2 a_3)y + a_1 c y^2 - 2cy\dot{y} = a_3 b u \tag{9}$$

3. Learning Control Design

Define the state vector as $x = [x_1, x_2]^T = [y, \dot{y}]^T \in \mathbb{R}^2$. Then the state equations corresponding to the nonlinear input–output Equation (9) can be expressed as

$$\begin{aligned} \dot{x}_1 &= x_2 \\ \dot{x}_2 &= f(x) + gu + d \end{aligned} \tag{10}$$

where

$$f(x) = (a_1 a_4 - a_2 a_3)x_1 + (a_1 + a_4)x_2 - a_1 c x_1^2 + 2c x_1 x_2, \; g = a_3 b \tag{11}$$

and $d \in \mathbb{R}$ (assumed bounded) represents the lumped uncertainties and disturbances. The objective now is to design a control law u such that tracking of a given reference trajectory $r(t) = [r_1(t), r_2(t)]^T$, where $r_2 = \dot{r}_1$, is achieved.

Define the tracking error variables

$$\begin{aligned} e_1 &= r_1 - x_1 \\ e_2 &= r_2 - x_2 \end{aligned} \tag{12}$$

Let $k = [k_1, k_2]^T \in \mathbb{R}^2, \; k_i > 0, \; i = 1, 2$ denote the control gain vector. We choose the input as

$$u = g^{-1}\left[-f(x) + k_1 e_1 + k_2 e_2 + \dot{r}_2 - \hat{d}\right] \tag{13}$$

where $\hat{d}$ is the disturbance estimate, so that the closed-loop error dynamics can be expressed as

$$\begin{aligned} \dot{e}_1 &= e_2 \\ \dot{e}_2 &= -k_2 e_2 - k_1 e_1 - d + \hat{d} \end{aligned} \tag{14}$$

3.1. Update Rules

The update rules ensure that the following expression that corresponds to the desired closed-loop error dynamics converges to zero:

$$s(e, k_d) = \dot{e}_2 + k_{2d}e_2 + k_{1d}e_1 \tag{15}$$

Here the gradient descent method is used to minimize the cost function (or closed-loop error function) given by

$$C = \frac{1}{2}(s(e, k_d))^2 \tag{16}$$

Note that $s(e, k_d)$ can be rewritten as

$$s(e, k_d) = -k_2e_2 - k_1e_1 - d + \hat{d} + k_{2d}e_2 + k_{1d}e_1 \tag{17}$$

Therefore, the time update rule for controller gains can be computed as

$$\dot{k}_i = -\alpha_i \frac{\partial C}{\partial k_i} = \alpha_i s(e, k_d)e_i \tag{18}$$

where $\alpha_i > 0$ is the ith controller gain's learning rate. Similarly, the time update rule for the disturbance estimate is

$$\dot{\hat{d}} = -\alpha_{\hat{d}} \frac{\partial C}{\partial \hat{d}} = -\alpha_{\hat{d}} s(e, k_d) \tag{19}$$

where $\alpha_{\hat{d}}$ is the learning rate for the disturbance estimate. The above strategy updates the controller gains and the disturbance estimate until the cost function reaches the global minimum at $C(e, k_d) = 0$.

3.2. Proof of Stability and Global Minimum

The closed-loop error dynamics given by Equation (14) can be expressed as

$$\ddot{e}_1 + k_2\dot{e}_1 + k_1e_1 + d - \hat{d} = 0 \tag{20}$$

Assuming that the rate of change of the disturbance is negligible compared to that of the error variables, we time differentiate Equation (14) with $\dot{d} = 0$ to obtain the following expression:

$$\dddot{e}_1 + k_2\ddot{e}_1 + (k_1 + \dot{k}_2)\dot{e}_1 + \dot{k}_1e_1 - \dot{\hat{d}} = 0 \tag{21}$$

Following our previous work in [30], we plug in the expressions for $\dot{k}_i$ and $\dot{\hat{d}}$ to obtain:

$$\dddot{e}_1 + a_1(z)\ddot{e}_1 + a_2(z)\dot{e}_1 + a_3(z)e_1 = 0, \tag{22}$$

where $z = [e_1\ \dot{e}_1\ \ddot{e}_1]^T$ and

$$\begin{aligned} &a_1(z) = k_2 + \alpha_{\hat{d}} + \beta(z), \quad a_2(z) = k_1 + k_{2d}(\alpha_{\hat{d}} + \beta(z)) \\ &a_3(z) = k_{1d}(\alpha_{\hat{d}} + \beta(z)), \quad \beta(z) = \alpha_1 z_1^2 + \alpha_2 z_2^2 \end{aligned} \tag{23}$$

Clearly, $a_i(z) > 0,\ \forall z,\ i = 1, 2, 3$, and the characteristic equation for $a_i(0),\ i = 1, 2, 3$, is given by

$$\lambda^3 + (k_2 + \alpha_{\hat{d}})\lambda^2 + (k_1 + \alpha_{\hat{d}}k_{2d})\lambda + k_{1d}\alpha_{\hat{d}} = 0 \tag{24}$$

We choose $k_i,\ k_{id}$, and $\alpha_{\hat{d}}$ such that the following condition is satisfied

$$k_{2d}\alpha_{\hat{d}}^2 + (k_1 + k_2k_{2d} - k_{1d})\alpha_{\hat{d}} + k_1k_2 > 0 \tag{25}$$

so that the roots of the characteristic Equation (24) satisfy the stability condition $\mathcal{R}\{\lambda_i\} < 0,\ i = 1, 2, 3$.

We now show that the simple learning strategy results in a global minimum. The second derivatives of the cost function Equation (16) can be computed as

$$\begin{aligned} \frac{\partial^2 C}{\partial k_i^2} &= -e_i \frac{\partial s}{\partial k_i} = e_i^2, \quad i = 1,2 \\ \frac{\partial^2 C}{\partial \hat{d}^2} &= \frac{\partial s}{\partial \hat{d}} = 1 \end{aligned} \tag{26}$$

Clearly, the sign of the curvature for the cost function remains positive and thus there do not exist any local minima, i.e., the closed-loop error dynamics reach the global minimum at $s(e, k_d) = 0$. This ensures that the controller gains ($k_i, \ i = 1,2$) and the disturbance estimate ($\hat{d}$) converge to finite values.

4. Simulation

In the throttling process, the mass flow rate needs to be kept at a certain level, to change instantly from one level to another (immediate decrease or increase), or to change linearly/nonlinearly, gradually and continually for a certain period. In this section, four different numerical simulation scenarios are considered to evaluate the effectiveness of the proposed nonlinear control strategy for an electric pump for liquid-propellant rocket engines.

- Scenario I: Maintaining the mass flow rate at a constant level.
- Scenario II: Step-wise increasing and decreasing of the mass flow rate.
- Scenario III: Time-varying increasing and decreasing of the mass flow rate.
- Scenario IV: Nonlinear time-varying increasing and decreasing of the mass flow rate.

In the first scenario (i.e., Scenario I), the appropriate control actions are generated by the developed nonlinear controller to maintain the mass flow rate at a constant level. In the second scenario (i.e., Scenario II), a step-wise signal is considered to demonstrate the capability of the generated control actions for adequately increasing and decreasing the mass flow rate. In the third scenario (i.e., Scenario III), the capability of the proposed nonlinear controller is additionally evaluated by tracking a time-varying signal. Ultimately, in the last scenario (i.e., Scenario IV), the capability of the proposed nonlinear controller is further evaluated by tracking a nonlinear time-varying signal. In this paper, we choose reference rotational speed n_r = 40,000 rpm and reference mass flow rate $\dot{m}_r = 1.35$ kg/s, and evaluate the system in the variable range of mass flow rate $\dot{m} \in [0, 1.35]$ kg/s similar to the range defined in [16]. In addition, we use the electric pump parameters given in [16].

$$\begin{aligned} a_1 &= -205.8824 \ 1/\mathrm{s}, & \mathrm{a}_2 &= -2.1902 \times 10^4 \ \mathrm{A/kg} \\ a_3 &= 1.7495 \times 10^4 \ \mathrm{kg/A/s}, & \mathrm{a}_4 &= -1000 \ 1/\mathrm{s} \\ b &= 1764.706 \ \mathrm{A/V/s}, & \mathrm{c} &= -2.2108 \times 10^7 \ 1/\mathrm{kg} \end{aligned} \tag{27}$$

The following platform is used for performing all the numerical analysis. We used a MacBook Pro (macOS 13.4.1) with Processor: 2.3 GHz Intel Core i5, and Memory: 16.00 GB. The total simulation time for all the scenarios is 100 seconds. In this work, to numerically solve the equations of the system, we used the Runge–Kutta 4th order algorithm, and the sampling time (T_s) of 0.05 s was considered.

All the parameters and their associated values used in these simulations are listed in Table 1.

Table 1. Numerical Simulation Parameters.

Parameter	Value	Parameter	Value	Parameter	Value
y_0	0	$k_1(0)$	0.1	$\hat{d}(0)$	0
$\dot{y}_0$	0	$k_2(0)$	0.1	$\alpha_{\hat{d}}$	2
k_{1d}	1	α_1	1	d	1
k_{2d}	2	α_2	1	T_s	0.05

4.1. Scenario I: Maintaining the Mass Flow Rate at a Constant Level

The first scenario (i.e., Scenario I) presents the evaluation of the developed nonlinear controller to maintain the mass flow rate at a constant level. To study this, we considered a constant trajectory (i.e., $\dot{m}_d = 1.25$), and the objective is for the controller to generate the appropriate control actions that minimize the tracking error.

Figure 2 shows the desired output and the actual output of the system under control for a constant trajectory considered in the first scenario. Figure 3 plots the generated control action for the system considering a constant trajectory tracking in Scenario I. Figure 2 clearly illustrates that the system output reaches the desired reference in a very short time with no overshoot. This demonstrates that the mass flow rate can be kept at a certain level using the developed nonlinear controller. Figure 3 shows that the generated control action is smooth and stable. This results in a smooth throttling process.

The calculated control gains (i.e., k_1 and k_2) and the estimated disturbance (i.e., $\hat{d}$) for the system in constant trajectory tracking in Scenario I (i.e., maintaining the mass flow rate at a constant level) are plotted in Figures 4 and 5, respectively. Figure 4 shows that both control gains (i.e., k_1 and k_2) converge to certain values, which results in a stable system under control. Figure 5 shows that the estimated disturbance converges to 1, which further demonstrates the capability of the developed nonlinear controller to estimate and compensate for the disturbance.

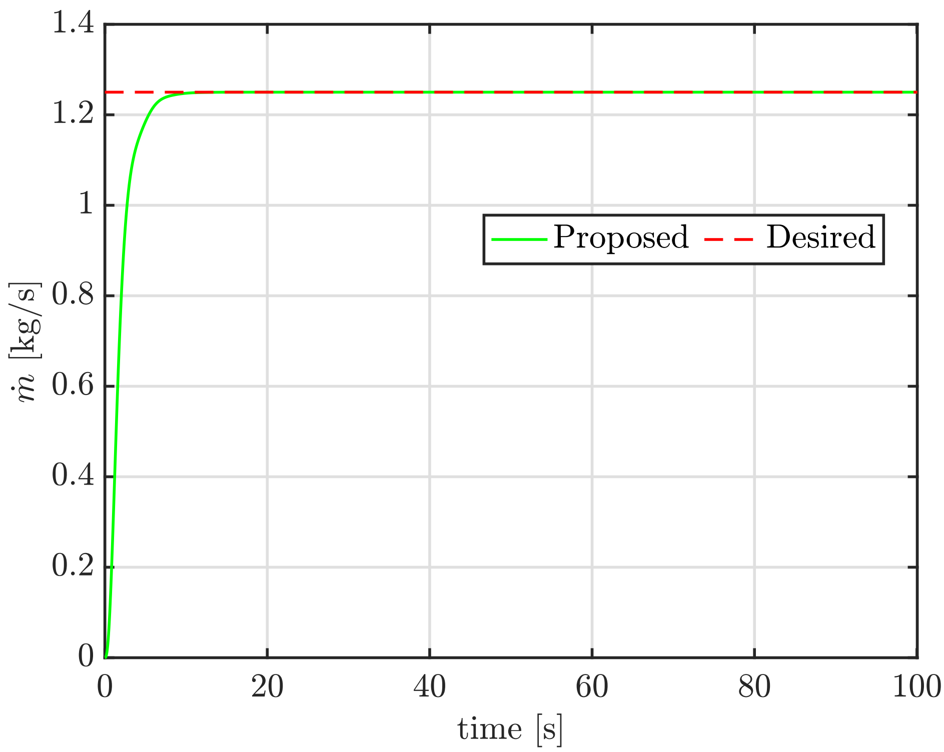

Figure 2. The desired and actual output of the system in constant trajectory tracking (see Scenario I: maintaining the mass flow rate at a constant level).

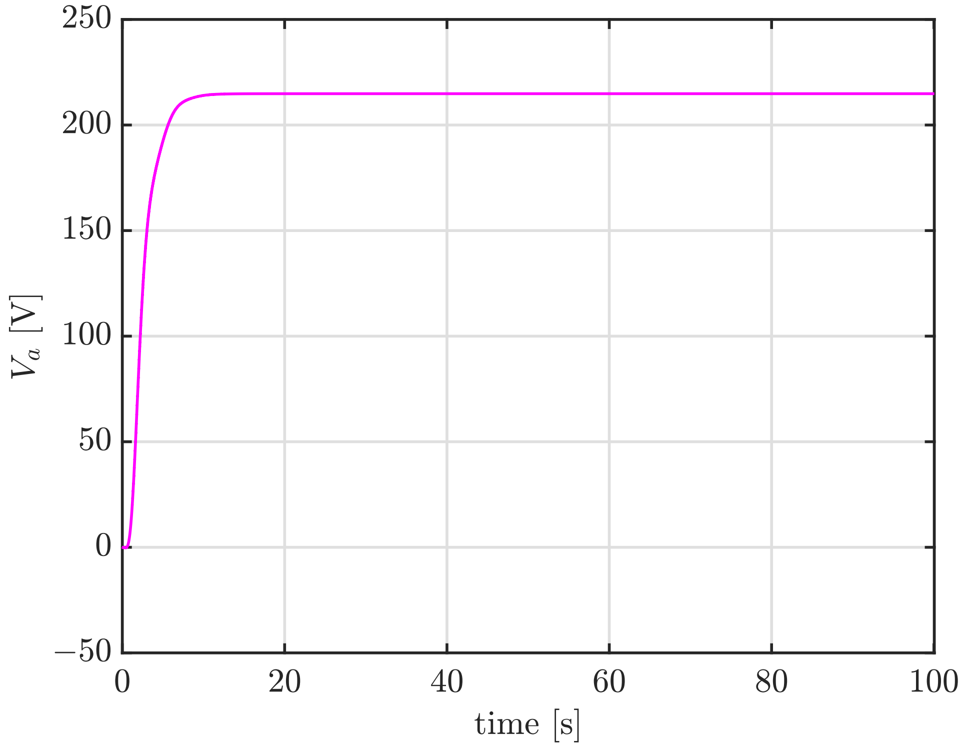

Figure 3. The generated control action for the system in constant trajectory tracking in Scenario I (maintaining the mass flow rate at a constant level).

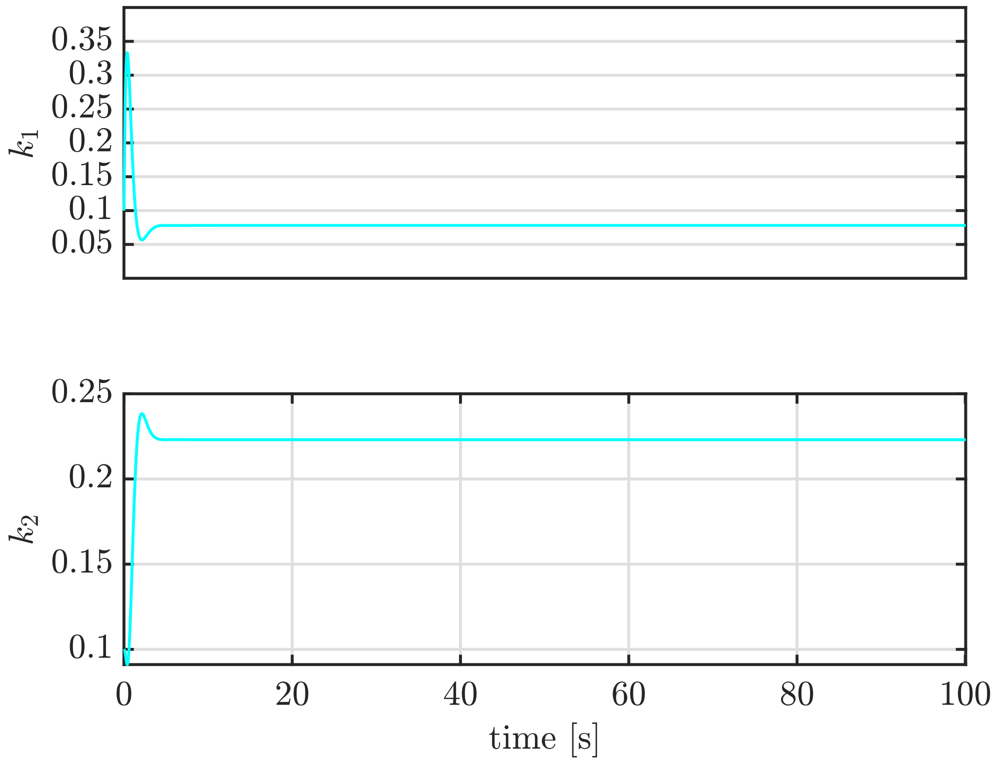

Figure 4. The calculated control gains for the system in constant trajectory tracking in Scenario I (maintaining the mass flow rate at a constant level).

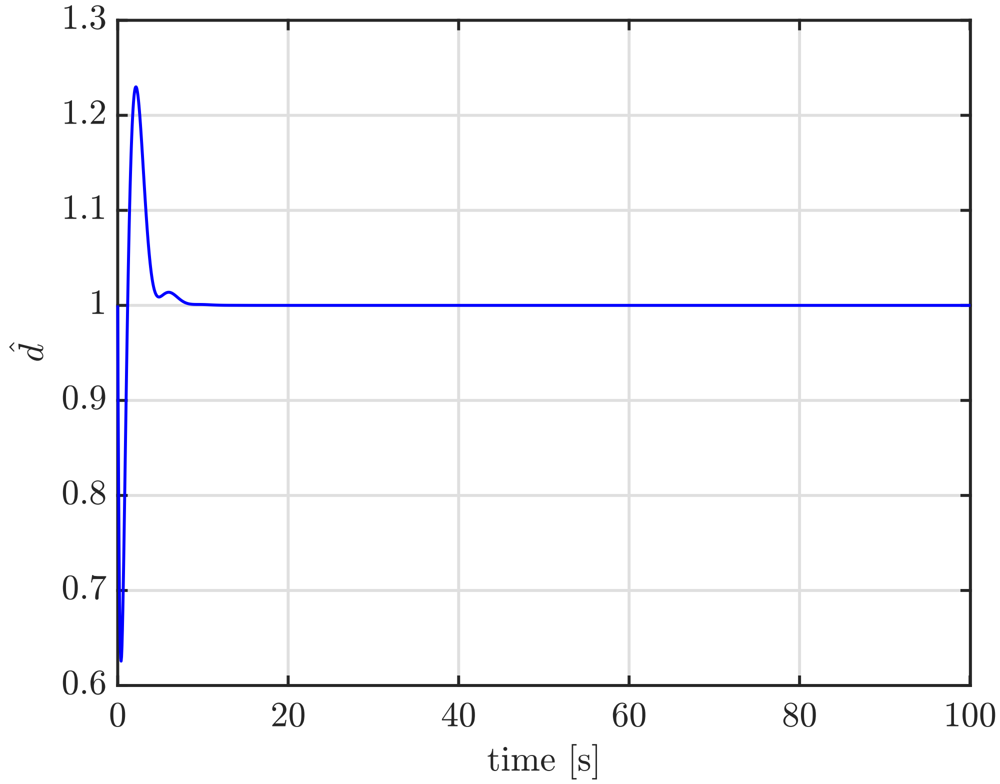

Figure 5. The estimated disturbance for the system in constant trajectory tracking in Scenario I (maintaining the mass flow rate at a constant level).

4.2. Scenario II: Step-Wise Increasing and Decreasing of the Mass Flow Rate

The second scenario (i.e., Scenario II) exemplifies the capability of the developed nonlinear robust controller when generating the control actions to adequately increase and decrease the mass flow rate. This is performed by designing a step-wise signal as follows:

$$\dot{m}_d(t) = \begin{cases} 0.5 & 0 \leq t < 15 \\ 1 & 15 \leq t < 30 \\ 1.25 & 30 \leq t < 45 \\ 1.35 & 45 \leq t < 70 \\ 1 & 70 \leq t < 85 \\ 0.25 & 85 \leq t \leq 100 \end{cases}$$

Figure 6 shows the desired output and the actual output of the system under control for a step-wise trajectory considered in the second scenario. Figure 7 plots the generated control action for the system considering step-wise trajectory tracking in Scenario II. It is shown that the controller is successful in generating the appropriate control actions that minimize the tracking error. This clearly illustrates that the system output reaches the desired reference in a very short time with no overshoot. It also successfully increases and decreases the mass flow rate in response to immediate changes. This demonstrates that the mass flow rate can be increased/decreased and kept at a certain level using the developed nonlinear controller. The generated control action is smooth and stable, which results in a smooth throttling process.

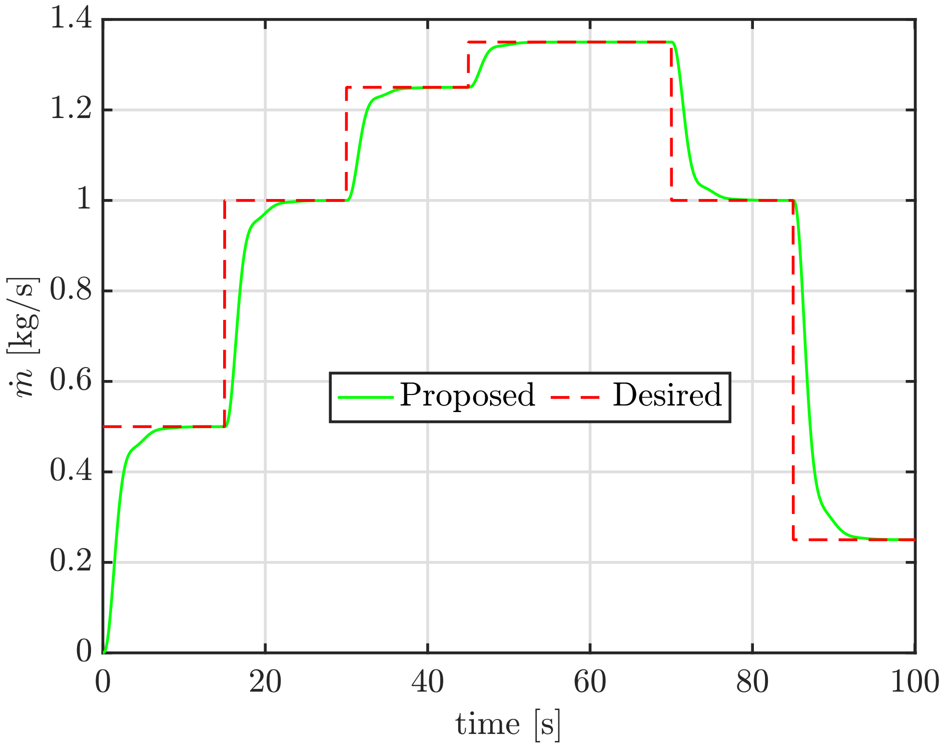

Figure 6. The desired and actual output of the system in step-wise trajectory tracking (see Scenario II: step-wise increasing and decreasing of the mass flow rate).

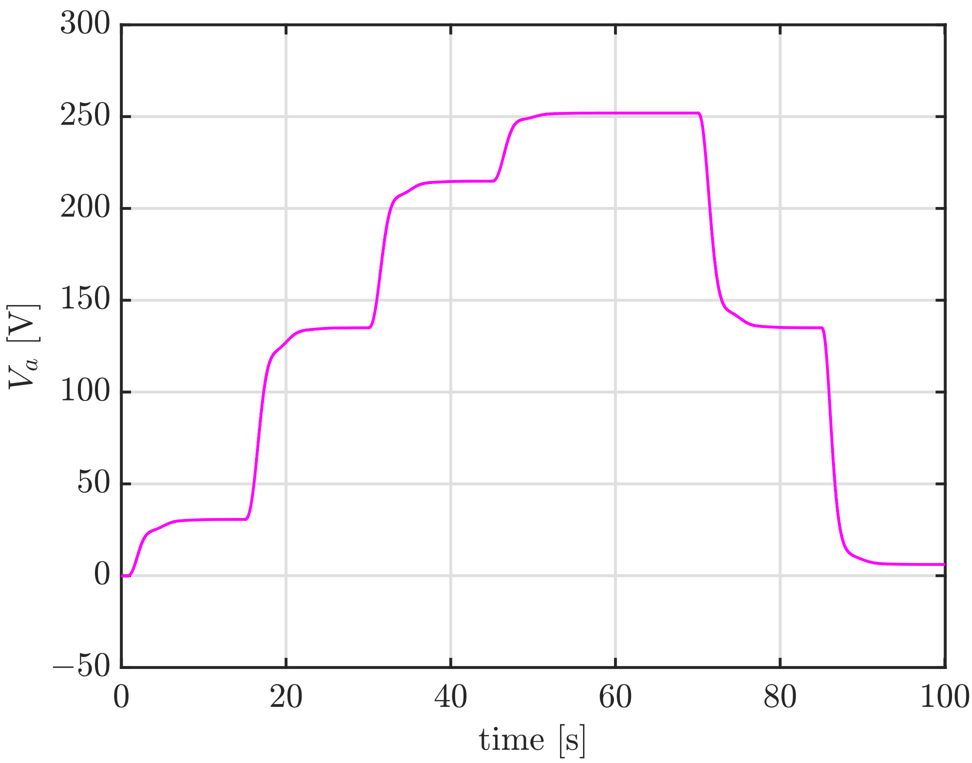

Figure 7. The generated control action for the system in step-wise trajectory tracking in Scenario II (step-wise increasing and decreasing of the mass flow rate).

The calculated control gains (i.e., k_1 and k_2) and the estimated disturbance (i.e., $\hat{d}$) for the system in step-wise trajectory tracking in Scenario II (i.e., step-wise increasing and decreasing of the mass flow rate) are plotted in Figures 8 and 9, respectively. Figure 8 shows that both control gains (i.e., k_1 and k_2) converge to certain values, which results in a stable system under control. These two gains change to compensate for the sudden changes imposed by changing the mass flow rate level. Figure 9 shows that the estimated disturbance converges to 1, which further demonstrates the capability of the developed nonlinear controller to estimate and compensate for the disturbance.

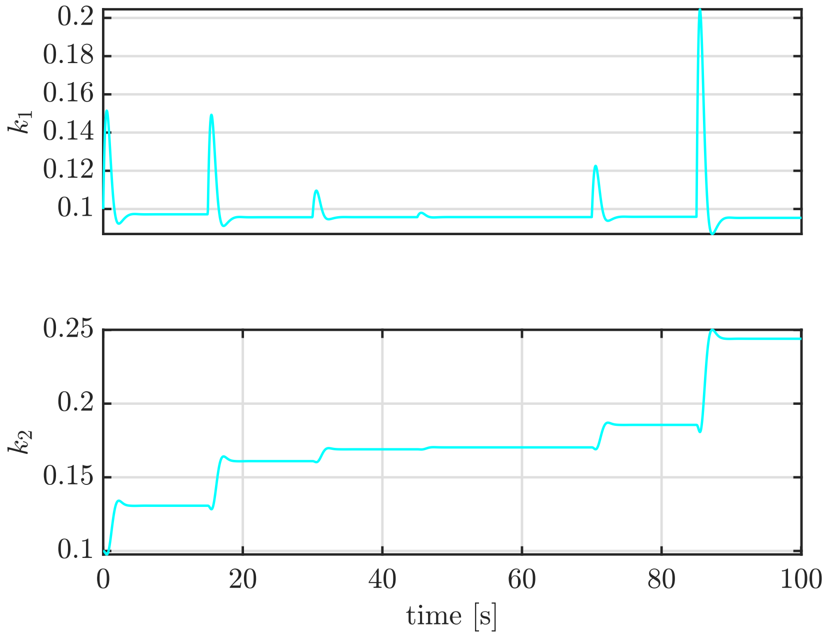

Figure 8. The calculated control gains for the system in step-wise trajectory tracking in Scenario II (step-wise increasing and decreasing of the mass flow rate).

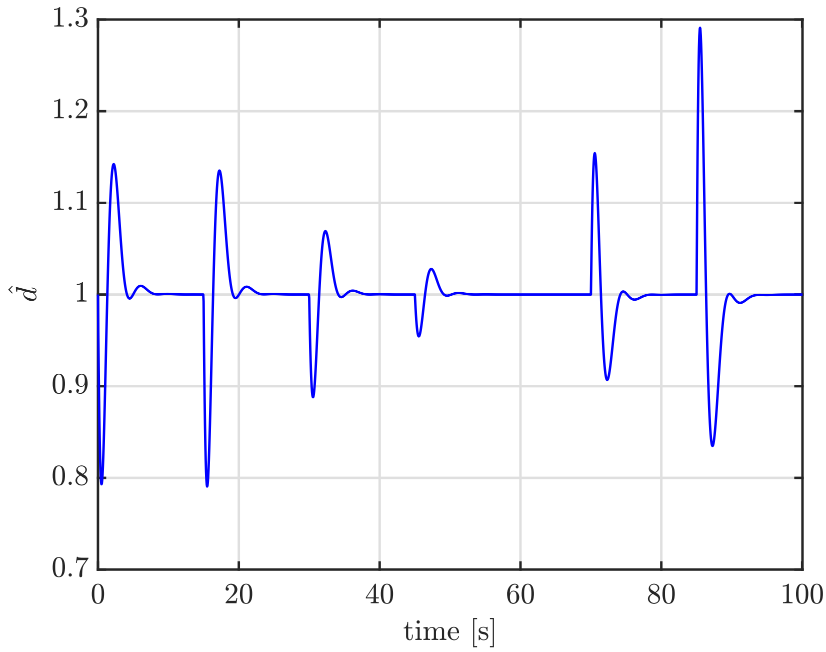

Figure 9. The estimated disturbance for the system in step-wise trajectory tracking in Scenario II (step-wise increasing and decreasing of the mass flow rate).

4.3. Scenario III: Time-Varying Increasing and Decreasing of the Mass Flow Rate

The third scenario (i.e., Scenario III) demonstrates the evaluation of the developed nonlinear robust controller when generating the control actions to satisfactorily track a time-varying signal. This is performed by designing a time-varying signal that increases and decreases the mass flow rate as follows:

$$\dot{m}_d(t) = \begin{cases} 0.05 \times t & 0 \leq t < 25 \\ 1.25 - 0.05 \times (t - 25) & 25 \leq t < 50 \\ 0.05 \times (t - 50) & 50 \leq t < 75 \\ 1.25 - 0.05 \times (t - 75) & 75 \leq t \leq 100 \end{cases}$$

Figure 10 shows the desired output and the actual output of the system under control for a time-varying trajectory considered in the third scenario. Figure 11 plots the generated control action for the system considering a time-varying trajectory tracking in Scenario III. It is illustrated that the controller successfully generates the appropriate control actions that minimize the tracking error. This clearly illustrates that the system output successfully follows the desired reference. It also linearly, gradually, and continually increases and decreases the mass flow rate in response to changes. This demonstrates that the mass flow rate can be increased/decreased using the developed nonlinear controller. The generated control action is smooth and stable, which results in a smooth throttling process.

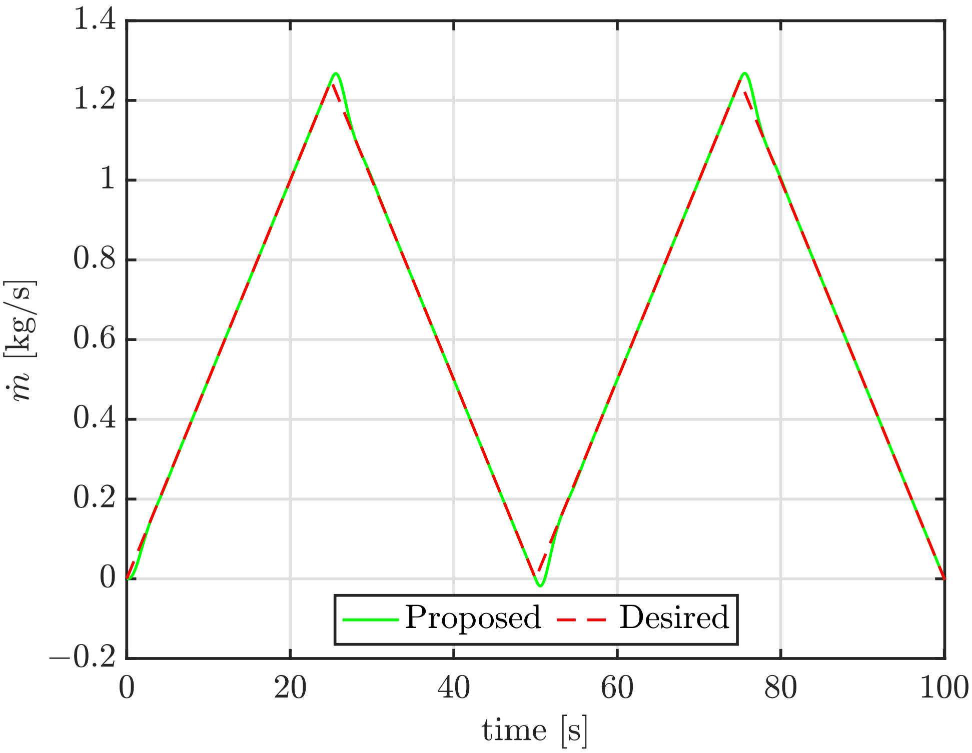

Figure 10. The desired and actual output of the system in time-varying trajectory tracking (see Scenario III: time-varying increasing and decreasing of the mass flow rate).

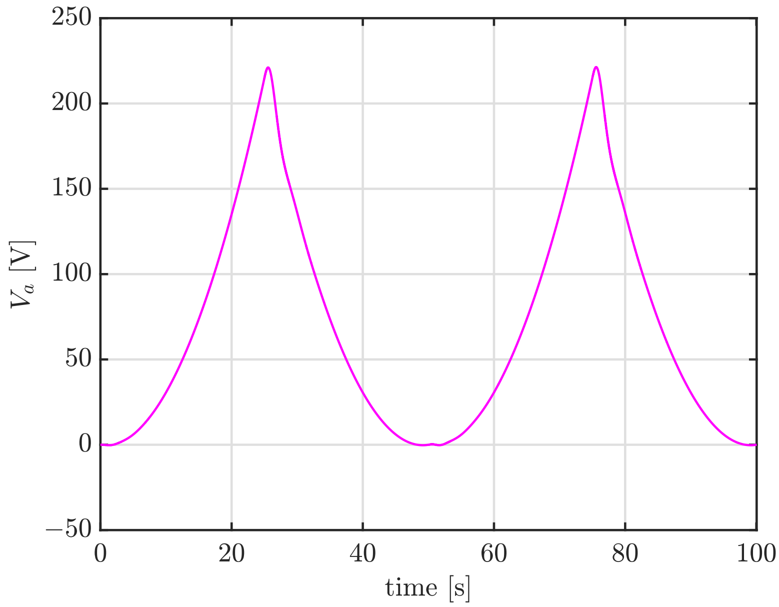

Figure 11. The generated control action for the system in time-varying trajectory tracking in Scenario III (time-varying increasing and decreasing of the mass flow rate).

The calculated control gains (i.e., k_1 and k_2) and the estimated disturbance (i.e., $\hat{d}$) for the system in a time-varying trajectory tracking in Scenario III (i.e., time-varying increasing and decreasing of the mass flow rate) are shown in Figures 12 and 13, respectively. Figure 12 shows that both control gains (i.e., k_1 and k_2) converge to certain values for each increasing/decreasing part of the desired signal, which results in a stable system under control. These two gains change to compensate for the sharp changes imposed by changing the mass flow rate at the peaks and valleys. Figure 13 shows that the estimated disturbance converges to 1, which further demonstrates the capability of the developed nonlinear controller to estimate and compensate for the disturbance.

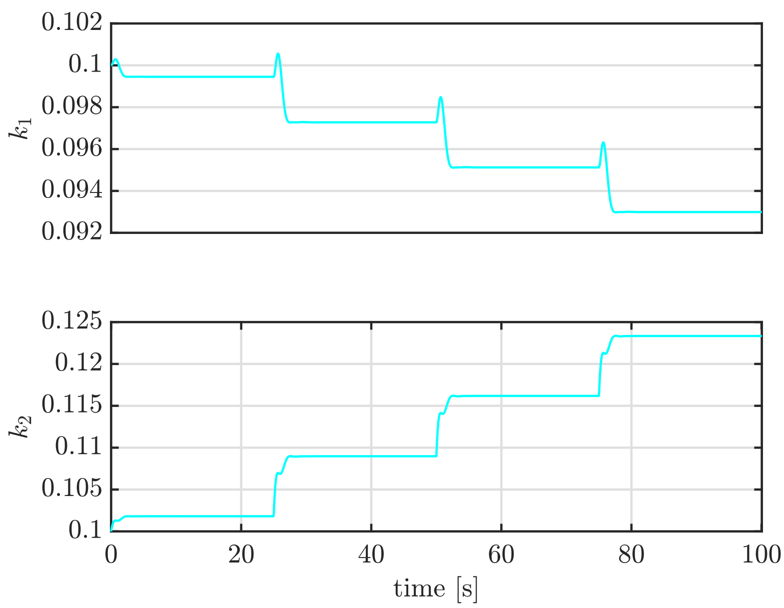

Figure 12. The calculated control gains for the system in time-varying trajectory tracking in Scenario III (time-varying increasing and decreasing of the mass flow rate).

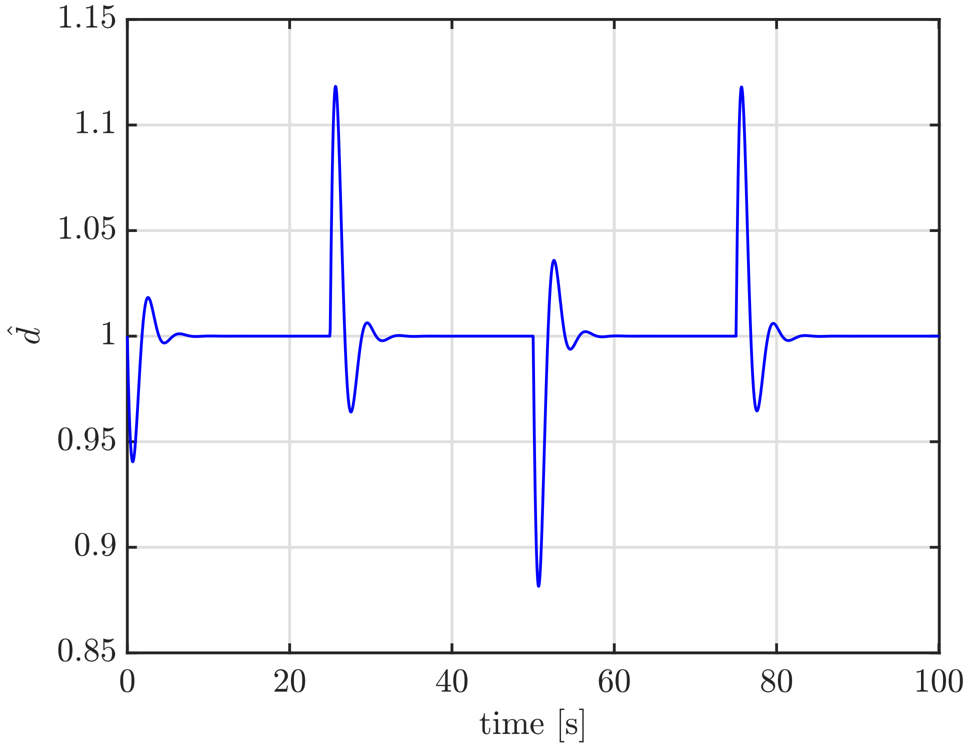

Figure 13. The estimated disturbance for the system in time-varying trajectory tracking in Scenario III (time-varying increasing and decreasing of the mass flow rate).

4.4. Scenario IV: Nonlinear Time-Varying Increasing and Decreasing of the Mass Flow Rate

The last scenario (i.e., Scenario IV) demonstrates the further evaluation of the developed nonlinear robust controller in generating the control actions for satisfactorily tracking a nonlinear time-varying signal. This is carried out by designing a nonlinear time-varying signal that increases and decreases the mass flow rate as follows:

$$\dot{m}_d(t) = 0.75 + 0.5 \times \cos(\frac{t}{8})$$

Figure 14 shows the desired output and the actual output of the system under control for a nonlinear time-varying trajectory considered in the last scenario. Figure 15 plots the generated control action for the system considering a nonlinear time-varying trajectory tracking in Scenario IV. It is illustrated that the controller successfully generates the appropriate control actions that minimize the tracking error. This clearly illustrates that the system output successfully follows the desired reference. It also nonlinearly, gradually, and continually increases and decreases the mass flow rate in response to changes. This demonstrates that the mass flow rate can be increased/decreased using the developed nonlinear controller. The generated control action is smooth and stable, which results in a smooth throttling process.

The calculated control gains (i.e., k_1 and k_2) and the estimated disturbance (i.e., $\hat{d}$) for the system in a nonlinear time-varying trajectory tracking in Scenario IV (i.e., nonlinear time-varying increasing and decreasing of the mass flow rate) are shown in Figures 16 and 17, respectively. Figure 16 shows that both control gains (i.e., k_1 and k_2) converge to certain values, which results in a stable system under control. Figure 17 shows that the estimated disturbance converges to 1, which further demonstrates the capability of the developed nonlinear controller to estimate and compensate for the disturbance.

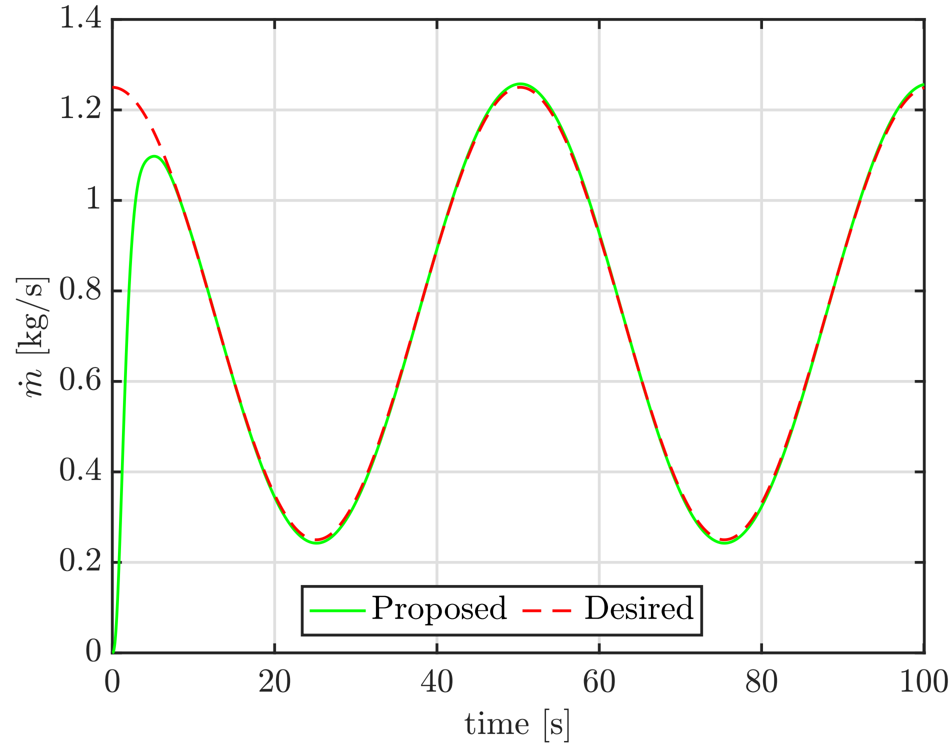

Figure 14. The desired and actual output of the system in nonlinear time-varying trajectory tracking (see Scenario IV: nonlinear time-varying increasing and decreasing of the mass flow rate).

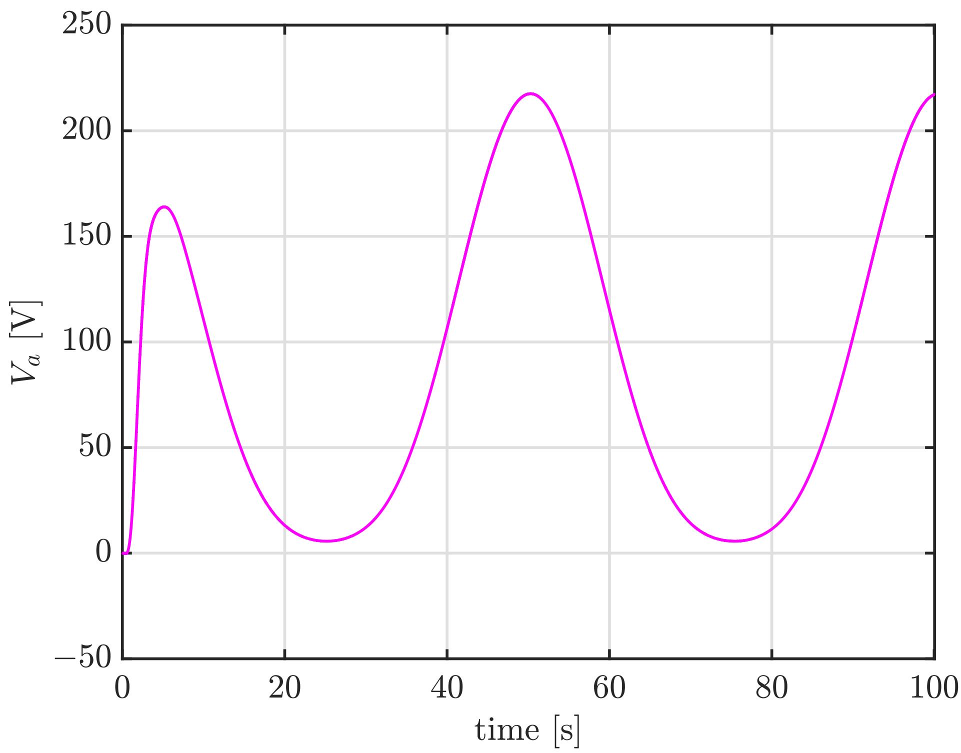

Figure 15. The generated control action for the system in time-varying trajectory tracking in Scenario IV (nonlinear time-varying increasing and decreasing of the mass flow rate).

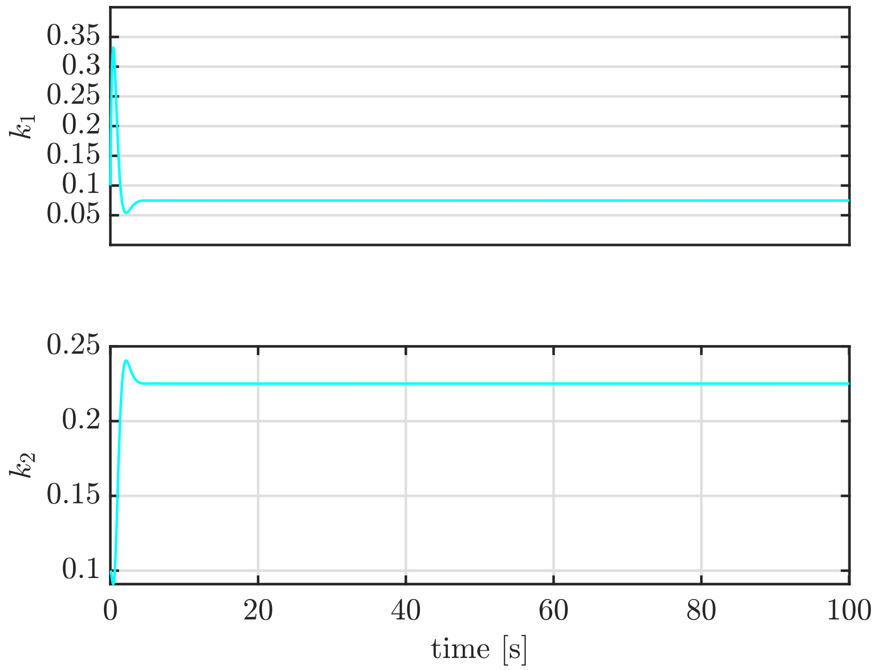

Figure 16. The calculated control gains for the system in nonlinear time-varying trajectory tracking in Scenario IV (nonlinear time-varying increasing and decreasing of the mass flow rate).

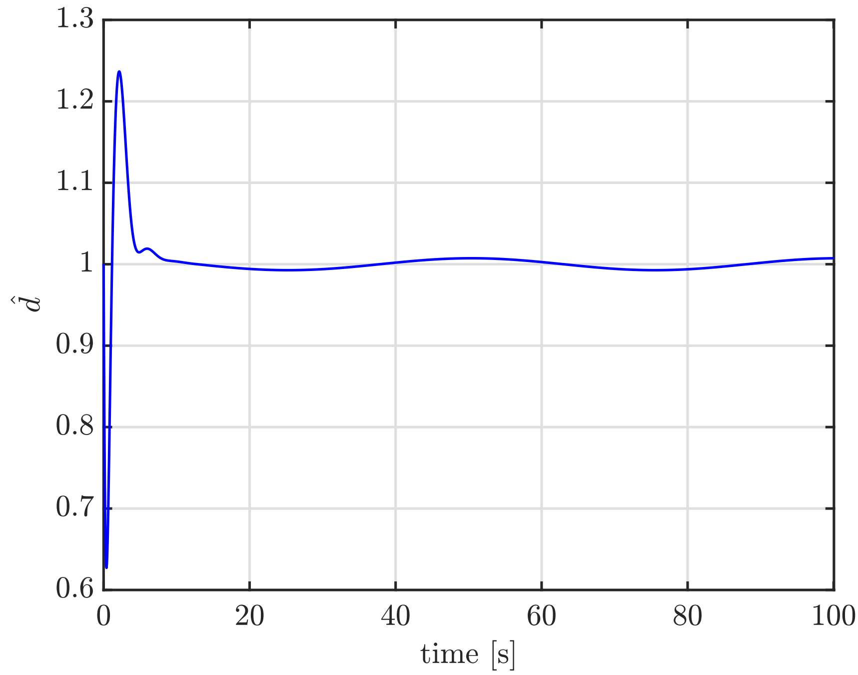

Figure 17. The estimated disturbance for the system in time-varying trajectory tracking in Scenario IV (nonlinear time-varying increasing and decreasing of the mass flow rate).

5. Conclusions and Extensions

A robust nonlinear control strategy for an electric pump for liquid-propellant rocket engines is presented. Compensating for the model uncertainties and disturbances, a simple learning control strategy is developed by minimizing the cost function defined on the error dynamics of the nonlinear system. A stability analysis for the nonlinear system is provided. To exemplify the effectiveness of the nonlinear control method, multiple numerical computer simulation results are considered. This is performed by applying the developed controller to an electric pump model consisting of a brushless permanent-magnet direct current (DC) motor and a centrifugal pump. This demonstrates that the mass flow rate can be increased/decreased and kept at a certain level using the developed nonlinear controller and the generated control actions are smooth and stable, which results in a smooth throttling process.

Author Contributions: M.R. performed the analysis and wrote the original draft. M.J. obtained the computational results and contributed to the editing of the manuscript. Z.K. helped with visualization. All authors have read and agreed to the published version of the manuscript.

Funding: This research received no external funding.

Data Availability Statement: Not applicable.

Acknowledgments: The first two authors wish to acknowledge the support provided by Columbus State University, Columbus, GA, USA.

Conflicts of Interest: The authors declare no conflict of interest.

Nomenclature

The following abbreviations are used in this manuscript:

R_a	Armature resistance	Ω
L_a	Armature inductance	mH
K_v	Motor back EMF constant	V/rad/s
K_t	Motor torque constant	N·m/A
J_m	Moment of inertia	kg·m^2
B_m	Viscous friction coefficient	N·m · s/rad
$\dot{m}$	Mass flow rate	kg/s
$\dot{m}_r$	Reference mass flow rate	kg/s
n	Rotational speed	rpm
n_r	Reference rotational speed	rpm
K	Pump constant	N·m· s^2/rad^2

References

1. Kwak, H.D.; Kim, D.J.; Kim, J.H.; gi Lee, H.; Choi, C.H.; Jeong, E.H. Liquid Rocket Engine Using Pump Driven by Electric Motor. U.S. Patent Application 15/750,776, 16 August 2018.
2. Rachov, P.P.; Tacca, H.; Lentini, D. Electric feed systems for liquid-propellant rockets. *J. Propuls. Power* **2013**, *29*, 1171–1180. [CrossRef]
3. Hong, S.S.; Kim, D.J.; Kim, J.S.; Choi, C.H.; Kim, J. Study on inducer and impeller of a centrifugal pump for a rocket engine turbopump. *Proc. Inst. Mech. Eng. Part C J. Mech. Eng. Sci.* **2013**, *227*, 311–319. [CrossRef]
4. Cui, P.; Li, Q.; Cheng, P.; Chen, L. System scheme design for LOX/LCH4 variable thrust liquid rocket engines using motor pump. *Acta Astronaut.* **2020**, *171*, 139–150. [CrossRef]
5. Liang, T.; Song, J.; Li, Q.; Cui, P.; Cheng, P.; Chen, L. System scheme design of electric expander cycle for LOX/LCH4 variable thrust liquid rocket engine. *Acta Astronaut.* **2021**, *186*, 451–464. [CrossRef]
6. Liang, T.; Cai, G.; Wang, J.; Gu, X.; Zhuo, L.; Cao, L. A hydrogen peroxide electric pump for throttleable hybrid rocket motor. *Acta Astronaut.* **2022**, *192*, 409–417. [CrossRef]
7. Kim, H.I.; Roh, T.S.; Huh, H.; Lee, H.J. Development of Ultra-Low Specific Speed Centrifugal Pumps Design Method for Small Liquid Rocket Engines. *Aerospace* **2022**, *9*, 477. [CrossRef]
8. Neill, T.; Judd, D.; Veith, E.; Rousar, D. Practical uses of liquid methane in rocket engine applications. *Acta Astronaut.* **2009**, *65*, 696–705. [CrossRef]
9. Zhou, C.; Yu, N.; Wang, J.; Cai, G. Starting and regulating characteristics of electric pump feed system for LRE under different schemes. *Appl. Sci.* **2022**, *12*, 6441. [CrossRef]
10. Johnsson, G.; Bigert, M. Development of small centrifugal pumps for an electric propellant pump system. *Acta Astronaut.* **1990**, *21*, 429–438. [CrossRef]
11. Waxenegger-Wilfing, G.; Hahn, R.; Deeken, J. Studies on electric pump-fed liquid rocket engines for micro-launchers. *Space Propuls.* **2018**, *452*.
12. Zhou, C.; Yu, N.; Wang, J.; Jiao, B.; Guo, X.; An, S. Design and analysis of rocket engine system with electric pump as subsystem. *J. Phys.* **2022**, *2369*, 012066. [CrossRef]
13. Lee, J.; Roh, T.S.; Huh, H.; Lee, H.J. Performance analysis and mass estimation of a small-sized liquid rocket engine with electric-pump cycle. *Int. J. Aeronaut. Space Sci.* **2021**, *22*, 94–107. [CrossRef]

14. Soldà, N.; Lentini, D. Opportunities for a liquid rocket feed system based on electric pumps. *J. Propuls. Power* **2008**, *24*, 1340–1346. [CrossRef]
15. Liu, Y.; Yang, J.; He, Y.; Ni, Z.; Wu, Y. Concept and Key Technology Analysis of Electric Pump-Fed Liquid Propellant Rocket Engine. *Conf. Ser. Earth Environ. Sci.* **2021**, *781*, 042016. [CrossRef]
16. Hu, R.; Ferrari, R.M.; Chen, Z.; Cheng, Y.; Zhu, X.; Cui, X.; Wu, J. System analysis and controller design for the electric pump of a deep-throttling rocket engine. *Aerosp. Sci. Technol.* **2021**, *114*, 106729. [CrossRef]
17. Zhou, C.; Yu, N.; Cai, G.; Wang, J. Comparison between the dynamic characteristics of electric pump fed engine and expander cycle engine. *Aerosp. Sci. Technol.* **2022**, *124*, 107508. [CrossRef]
18. Young, K.D.; Utkin, V.I.; Ozguner, U. A control engineer's guide to sliding mode control. *IEEE Trans. Control. Syst. Technol.* **1999**, *7*, 328–342. [CrossRef]
19. Hewing, L.; Wabersich, K.P.; Menner, M.; Zeilinger, M.N. Learning-based model predictive control: Toward safe learning in control. *Annu. Rev. Control. Robot. Auton. Syst.* **2020**, *3*, 269–296. [CrossRef]
20. Hagan, M.T.; Demuth, H.B. Neural networks for control. In Proceedings of the 1999 American Control Conference (Cat. No. 99CH36251), San Diego, CA, USA, 2–4 June 1999; IEEE: New York, NY, USA, 1999; Volume 3, pp. 1642–1656.
21. King, P.J.; Mamdani, E.H. The application of fuzzy control systems to industrial processes. *Automatica* **1977**, *13*, 235–242. [CrossRef]
22. Krener, A. Feedback linearization. In *Mathematical Control Theory*; Springer: New York, NY, USA, 1999; pp. 66–98.
23. Madani, T.; Benallegue, A. Backstepping control for a quadrotor helicopter. In Proceedings of the 2006 IEEE/RSJ International Conference on Intelligent Robots and Systems, Beijing, China, 9–15 October 2006; IEEE: New York, NY, USA, 2006; pp. 3255–3260.
24. Jafari, M.; Xu, H. A biologically-inspired intelligent controller for distributed velocity control of multiple electro-hydraulic servo-systems. In Proceedings of the 2017 IEEE Symposium Series on Computational Intelligence (SSCI), Honolulu, HI, USA, 27 November–1 December 2017; IEEE: New York, NY, USA, 2017; pp. 1–7.
25. Khanesar, M.A.; Kayacan, E.; Reyhanoglu, M.; Kaynak, O. Feedback error learning control of magnetic satellites using type-2 fuzzy neural networks with elliptic membership functions. *IEEE Trans. Cybern.* **2015**, *45*, 858–868. [CrossRef]
26. Hajimani, M.; Gholami, M.; Dashti, Z.A.S.; Jafari, M.; Shoorehdeli, M.A. Neural adaptive controller for magnetic levitation system. In Proceedings of the 2014 Iranian Conference on Intelligent Systems (ICIS), Bam, Iran, 4–6 February 2014; IEEE: New York, NY, USA, 2014; pp. 1–6.
27. Stebler, S.; Campobasso, M.; Kidambi, K.; MacKunis, W.; Reyhanoglu, M. Dynamic neural network-based sliding mode estimation of quadrotor systems. In Proceedings of the 2017 American Control Conference (ACC), Seattle, WA, USA, 24–26 May 2017; IEEE: New York, NY, USA, 2017; pp. 2600–2605.
28. Mehndiratta, M.; Kayacan, E.; Reyhanoglu, M.; Kayacan, E. Robust tracking control of aerial robots via a simple learning strategy-based feedback linearization. *IEEE Access* **2019**, *8*, 1653–1669. [CrossRef]
29. Reyhanoglu, M.; Jafari, M.; Rehan, M. Simple learning-based robust trajectory tracking control of a 2-DOF helicopter system. *Electronics* **2022**, *11*, 2075. [CrossRef]
30. Reyhanoglu, M.; Jafari, M. A Simple Learning Approach for Robust Tracking Control of a Class of Dynamical Systems. *Electronics* **2023**, *12*, 2026. [CrossRef]